Journal of Colloid and Interface Science 392 (2013) 206–212

Contents lists available at SciVerse ScienceDirect

Journal of Colloid and Interface Science

www.elsevier.com/locate/jcis

# Hydrothermal synthesis and upconversion luminescence properties of β-$NaGdF_4$:$Yb^{3+}$/$Tm^{3+}$ and β-$NaGdF_4$:$Yb^{3+}$/$Ho^{3+}$ submicron crystals with regular morphologies

Jing Li [a,c], Zhendong Hao [a], Xia Zhang [a], Yongshi Luo [a], Jihong Zhao [b], Shaozhe Lü [a], Jian Cao [a,c], Jiahua Zhang [a,*]

[a] State Key Laboratory of Luminescence and Applications, Changchun Institute of Optics, Fine Mechanics and Physics, Chinese Academy of Sciences, 3888 Eastern South Lake Road, Changchun 130033, China
[b] Jilin Cancer Hospital, 1018 Huguang Road, Changchun 130012, China
[c] Graduate School of Chinese Academy of Sciences, Beijing 100039, China

ARTICLE INFO

*Article history:*
Received 20 July 2012
Accepted 12 September 2012
Available online 22 October 2012

*Keywords:*
Hexagonal prisms
EDTA
β-$NaGdF_4$
Hydrothermal synthesis
UCL properties
$Yb^{3+}$/$Tm^{3+}$
$Yb^{3+}$/$Ho^{3+}$

ABSTRACT

Single phase β-$NaGdF_4$:$Yb^{3+}$/$Tm^{3+}$ and β-$NaGdF_4$:$Yb^{3+}$/$Ho^{3+}$ submicron crystals with various morphologies including hexagonal prisms, spindles, and spheres were synthesized via the one-step hydrothermal method by controlling the pH values and sort of chelators (EDTA and citric acid). The prepared products showed intense up-converted luminescence (UCL) pumped by infrared laser at 980 nm. The hexagonal prisms that meaning high degree crystallinity demonstrated strong UCL in comparison with other morphologies such as spindles and spheres. In β-$NaGdF_4$:$Yb^{3+}$/$Tm^{3+}$, UCL not only appeared transitions from $^1G_4$, $^1D_2$, and $^1I_6$ states to the lower lying states of $Tm^{3+}$, but also $^6P_J \rightarrow {}^8S_{7/2}$ transition (310 nm) of $Gd^{3+}$. These UCL were responsible for three, five, and six photons processes determined by pump power dependence of UCL intensities. The observation of UCL of $Gd^{3+}$ implied occurrence of energy transfer from $Tm^{3+}$:$^1I_6$ to $Gd^{3+}$:$^6P_J$.



## 1. Introduction

Over the past decades, the infrared to visible up-converted luminescence (UCL) in rare earth ions doped crystals have been extensively studied due to their potential applications in biological fluorescent labels, color displays, and infrared sensors [1–4]. Among them, Lanthanide ($Ln^{3+}$) fluoride compounds β-$NaYF_4$ and β-$NaGdF_4$ act as proper hosts for achieving highly bright UCL because they exhibit low phonon energies, high refractive indices, and high chemical stabilities. Considerable studies have shown that rare earth doped β-$NaYF_4$ is the very efficient UCL material [5–9], and various morphologies of which including hexagonal prisms [5,7,10], rods [6,9,11], and spheres [5,12,13] have been obtained by various synthetic methods. The β-$NaGdF_4$ host exhibits not only highly bright UCL [14], but also good magnetic characteristics [15–17], demonstrating both optical and magnetic functions for use in bioimaging rather than β-$NaYF_4$. And, $NaGdF_4$ is an ideal host material for ultraviolet (UV) quantum cutting phosphor [15,18,19]. However, there are only a few reports on synthesis of rare earth ion doped β-$NaGdF_4$ high degree crystallinity submicron crystals, compared to the nanoparticles [14,15,18,20]. And, submicron crystals with novel morphologies have the more remarkable effect than nanoparticles on the understanding of the crystal growth processes and potential technological applications in microelectronic devices [7,15,18]. The properties of microcrystalline powder can be greatly affected by the crystal shapes. Wang et al. [15] synthesized disk-like submicron β-$NaGdF_4$:$Yb^{3+}$/$Er^{3+}$ crystals by hydrothermal (HT) method using citric acid as the chelator. The prominent luminescence and paramagnetic properties of the prepared materials were studied. And, Wu et al. [18] prepared multiform morphologies β-$NaGdF_4$ by changing the $F^-$ sources and pH values, but unfortunately found only irregular submicroparticles due to the insufficient complexing ability of chelator and lack of equilibrium of chelator and pH value.

In general, the achievement of submicron β-$NaYF_4$ crystals with hexagonal prism morphology is the indication of high degree crystallinity [5,32], but the regular hexagonal prisms of submicron β-$NaGdF_4$ which have intense UCL have not been synthesized by HT method. On chelators for HT synthesis, besides citric acid, ethylenediamine tetraacetic acid (EDTA) is also an alternative because its chelate constant and structure stability coefficient are much larger than citric acid [21]. But EDTA-assisted HT for preparing the $NaGdF_4$ crystals with controlled morphologies has not been reported. It is therefore a significant research to use EDTA as the chelator to synthesize β-$NaGdF_4$, compared with citric acid.

* Corresponding author. Fax: +86 431 8617 6317.
*E-mail address:* zhangjh@ciomp.ac.cn (J. Zhang).

0021-9797/$ - see front matter © 2012 Elsevier Inc. All rights reserved.
http://dx.doi.org/10.1016/j.jcis.2012.09.076

In this paper, we reported HT synthesis of β-$NaGdF_4$:$Yb^{3+}$/$Tm^{3+}$ and β-$NaGdF_4$:$Yb^{3+}$/$Ho^{3+}$ submicron crystals and their UCL properties. In the synthesis, EDTA was applied to use as the chelator compared with citric acid. Regular morphologies including submicron hexagonal prisms (high crystallinity), spheres, and spindles were achieved by adjusting the pH values in aqueous solution strictly. The UCL processes of $Tm^{3+}$, $Gd^{3+}$, and $Ho^{3+}$ sensitized by $Yb^{3+}$ were discussed in β-$NaGdF_4$ host.

## 2. Experimental

### 2.1. Sample preparation

The synthesis of β-$NaGdF_4$:$Ln^{3+}$ ($Ln^{3+}$ = $Yb^{3+}$, $Tm^{3+}$ or $Ho^{3+}$) submicron crystals by the HT approach was described as follows: the appropriate amounts of $Gd_2O_3$ (4 N), $Yb_2O_3$ (4 N), $Tm_2O_3$ (4 N), and $Ho_2O_3$ (4 N) powders were dissolved in dilute nitric acid, respectively, to obtain 0.1 M Gd $(NO_3)_3$, 0.1 M Yb$(NO_3)_3$, 0.001 M Tm$(NO_3)_3$, and 0.02 M Ho$(NO_3)_3$ solutions. Then, the aqueous solutions containing $Gd^{3+}$, $Yb^{3+}$, $Tm^{3+}$/$Ho^{3+}$ with corresponding mole ratios were mixed and stirred to form homogeneous solutions at room temperature. In a typical procedure for the preparation of 0.5 mmol β-$NaGdF_4$:$Ln^{3+}$ ($Ln^{3+}$ = $Yb^{3+}$, $Tm^{3+}$ or $Ho^{3+}$), EDTA (0.1861 g) or citric acid (0.2102 g) as the chelator was added into the aforementioned solutions to form the white complex of metal-chelating with the molar ratio of EDTA/$Ln^{3+}$ of 1:1 or citric acid/$Ln^{3+}$ of 2:1. After vigorous stirring was continuously applied for 30 min, 0.2519 g of NaF was added into the complex as $F^-$ source under the molar ratio of $F^-$/$Ln^{3+}$ of 12:1. Then, the pH value of the mixed solution was adjusted to an appropriate constant by adding dropwise diluted NaOH or $HNO_3$ solution, which was a key factor to the morphology of product. After vigorous stirring for 2 h, the milky colloidal solution was transferred into a closed Teflon-lined stainless steel autoclave with 50.0 mL capacity and heated at 180 °C for 2 h. After the autoclave was cooled to room temperature naturally, the precipitates were collected by centrifugation at high speed of 8000 r/min and washing several times with deionized water and absolute ethanol. Then, the powder was obtained after being dried in a vacuum oven at 65 °C for 12 h. Table 1 shows the specific reaction conditions of HT synthesis and characteristics of the powders.

### 2.2. Measurements and characterization

Powder X-ray diffraction (XRD) data were collected using Cu Kα radiation ($\lambda$ = 1.54056 Å) on a Bruker D8 advance diffractometer equipped with a linear position-sensitive detector (PSD-50 m, M. Braun), operating at 40 kV and 40 mA with a step size of 0.01° ($2\theta$) in the range of 10–65°. The morphology was investigated by using field emission scanning electron microscopy (FE-SEM) (Hitachi S-4800). The transmission electron microscopy (TEM) and high-resolution transmission electron microscopy (HRTEM) images were performed using a JEOL JEM 2100 TEM equipped with an electron diffractometer (ED). The UCL spectra were measured using HITACHI F-4500 spectrometer pumped with a power-controllable 980 nm diode laser.

## 3. Results and discussion

### 3.1. Phase control

In our previous work, the products for low $F^-$/$Ln^{3+}$ values (⩽10:1) are mixtures of the orthorhombic phase $GdF_3$ and hexagonal phase β-$NaGdF_4$. As increasing $F^-$/$Ln^{3+}$ value up to 12:1, pure β-$NaGdF_4$ is achieved. Fig. 1 shows XRD patterns of the products synthesized by HT at 180 °C 2 h using EDTA (a) and citric acid (b) as the chelators for fixed $F^-$/$Ln^{3+}$ of 12:1 in aqueous solution with pH = 5. The pure hexagonal phase β-$NaGdF_4$ (JCPDS 27-0699) is achieved for samples synthesized using EDTA and citric acid as the chelators. We note that the HT synthesized β-$NaGdF_4$ in these conditions show enhanced (1 1 0) XRD peaks in comparison with the standard card of β-$NaGdF_4$. This result implies the presence of preferred growth direction dependent on morphology of the product. To obtain ideal XRD patterns of β-$NaGdF_4$ crystals, we fixed citric acid as the chelator and synthesized series β-$NaGdF_4$ products by adjusting pH values in the range of 4.8–9.0. It is significantly observed that the XRD patterns of the products gradually approach to the standard card of β-$NaGdF_4$ with increasing the pH values and the XRD pattern is finally identical to the standard card as pH = 9.0, as shown in Fig. 2. The corresponding morphologies of the β-$NaGdF_4$ crystals synthesized for pH values of 4.8, 5.0, 7.0, and 9.0 are illustrated in the SEM images (a–d), respectively in Fig. 3.

### 3.2. Morphology

When the pH was 4.8, the morphology of short hexagonal prism was formed, as shown in Fig. 3a. The synthesized short hexagonal prisms have an average size of 1 μm. A large quantity of regular short hexagonal prisms was obtained as the pH value increased up to 5, as shown in Fig. 3b. This indicates that the sufficient coordination between pH and citrate anion is responsible for the uniform morphology. In average, each hexagonal prism has the well-defined crystallographic facets with the side length of 500 nm and thickness of 600 nm. As the pH was further increased, the morphology of crystals had a significant change. The short hexagonal prisms changed to spheres as the pH value was 7, as shown in Fig. 3c. These spheres are uniform with diameter of 500 nm. The

**Table 1**
Characteristics of samples with various conditions in the HT processes.

| Chelator | Chelator/$Ln^{3+}$ | pH | Phase | Size | Morphology | Graph |
|---|---|---|---|---|---|---|
| Citric acid | 2:1 | 4.8 | Hexagonal | *L*: 1 μm<br>*H*: 1 μm | Hexagonal prisms | Fig. 3a |
| Citric acid | 2:1 | 5 | Hexagonal | *L*: 500 nm<br>*H*: 600 nm | Hexagonal prisms | Fig. 3b |
| Citric acid | 2:1 | 7 | Hexagonal | *D*: 500 nm | Spheres | Fig. 3c |
| Citric acid | 2:1 | 9 | Hexagonal | *D*: 400 nm | Spheres | Fig. 3d |
| EDTA | 1:1 | 4.5 | Hexagonal | *H*: 300 nm | Hexagonal prisms | Fig. 4a |
| EDTA | 1:1 | 5.1 | Hexagonal | *L*: 200 nm<br>*H*: 700 nm | Hexagonal prisms | Fig. 4b |
| EDTA | 1:1 | 7 | Hexagonal | *H*: 500 nm | Spindles | Fig. 4c |
| EDTA | 1:1 | 9 | Hexagonal | *H*: 400 nm | Spindles | Fig. 4d |

*D*: diameter; *H*: height; *L*: side length.

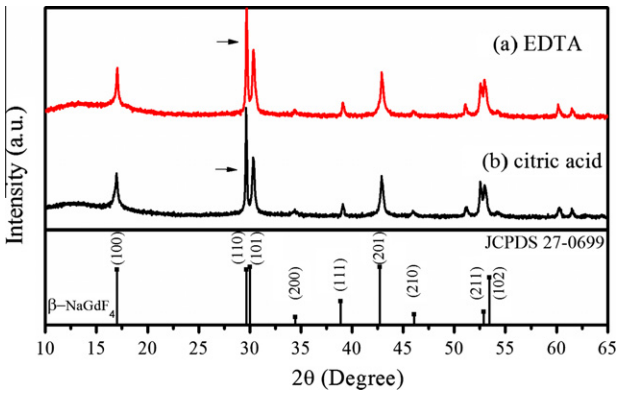


**Fig. 1.** XRD patterns of samples synthesized using EDTA (a) and citric acid (b) as the chelators for fixed pH value of 5 and molar ratio $F^-/Ln^{3+}$ of 12:1.

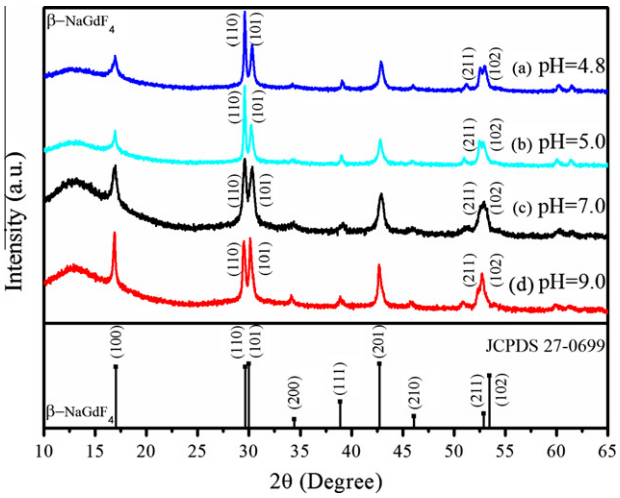


**Fig. 2.** XRD patterns of samples synthesized using citric acid as the chelator for fixed $F^-/Ln^{3+}$ ratio of 12:1 and pH value of 4.8 (a), 5 (b), 7 (c), and 9 (d).

surfaces of these spheres are coarse and contain nanosized substructures. With the pH was further increased to 9, the spheres had no further changes in morphology, but the surfaces of the spheres were smoother (inset of Fig. 3d). The morphologies changed from hexagonal prisms to spheres with increasing pH values can give an explanation why the XRD patterns show the enhanced (1 1 0) peak for low pH values and normal height of (1 1 0) peak for high pH values. Hexagonal prisms show geometrically non-isotropic shapes which have the preferred growth directions, resulting in stronger (1 1 0) XRD peak. Differently, spherical particles have isotropic structures without priority orientation that reasonably give a XRD pattern identical to the standard card of β-$NaGdF_4$, as shown in Fig. 2. The exact mechanism of citric acid for the change of morphology of β-$NaGdF_4$ is unclear to us at the moment. It may be explained that the function of citrate anions is different for controlling the relative growth rates along various crystallographic directions with the increase in the pH value. The crystal growth process will be discussed later.

EDTA is other efficient chelator for controlling the crystal morphology [13,22]. The chelate constant is much larger for EDTA ($lg\beta$ = 18–19) than citric acid ($lg\beta$ = 8–9) [22,23]. The structure stability coefficient of EDTA with $Ln^{3+}$ ions is larger than citric acid, because of its six binding sites (four binding sites in citric acid) and ring-like space structure [5].

For comparison with citric acid, EDTA is selected as the chelator to synthesize β-$NaGdF_4$ samples at 180 °C for 2 h with fixed $F^-/Ln^{3+}$ ratio of 12:1 and various pH values in the range of 4.5–9. The corresponding morphologies of the products are illustrated in Fig. 4. When the pH value was 4.5, spindles particles were formed, with an average length of about 300 nm and diameter of 100 nm in the middle. The convex structures at the center of the top and bottom facets demonstrate that the growth rate in the [0 0 1] direction is faster than the growth sideways in the [1 0 0] orientations in the condition EDTA existed. As the pH reached 5.1, highly uniform and mono-dispersed long hexagonal prisms were formed with a uniform side length of 200 nm and height of 700 nm, as shown in Fig. 4b (inset). The EDTA as the chelator facilitates longitudinal growth of β-$NaGdF_4$ sample. As the pH was further increased to 7, some long hexagonal prisms changed to the spindles again, as illustrated in Fig. 4c. When the pH reached to 9, the morphology was only the spindles with about 150 nm width in the middle and 400 nm height, as shown in Fig. 4d. The as-prepared spindles are other kind of cluster assembled from many primary nanocrystals, resulting

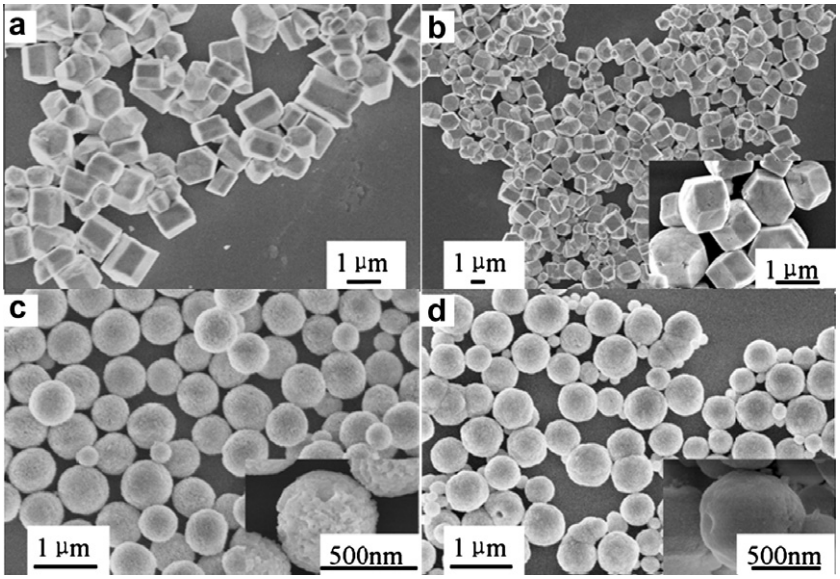


**Fig. 3.** The SEM images of β-$NaGdF_4$ submicron crystals synthesized using citric acid as the chelator for fixed $F^-/Ln^{3+}$ ratio of 12:1 and pH value of 4.8 (a), 5 (b), 7 (c), and 9 (d).

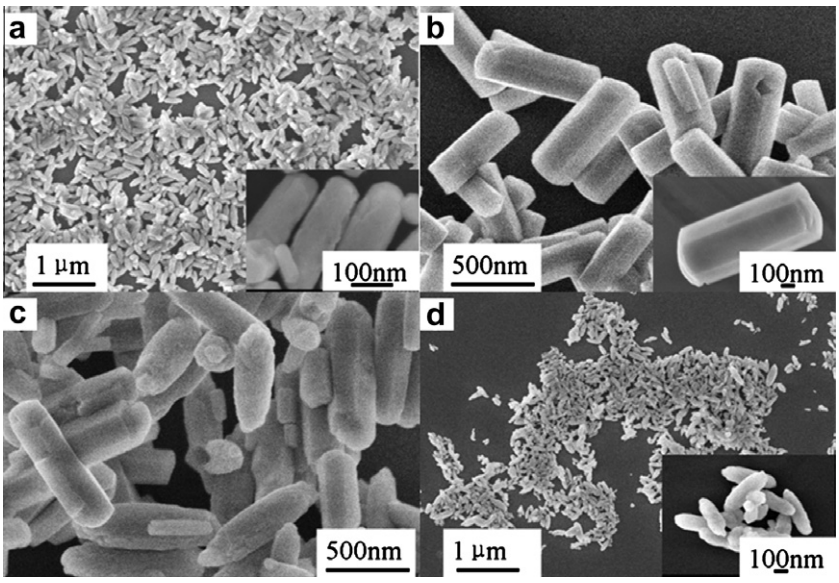


**Fig. 4.** The SEM images of β-$NaGdF_4$ submicron crystals prepared using EDTA as the chelator for fixed $F^-/Ln^{3+}$ ratio of 12:1 and pH value of 4.5 (a), 5.1 (b), 7 (c), and 9 (d).

the roughened surfaces (inset of Fig. 4d). All submicron crystals are synthesized above that are composed of lanthanide dopants 20%$Yb^{3+}$ and 0.3%$Tm^{3+}$. The morphologies are usually not affected by the dopants.

Fig. 5a exhibits a typical TEM image of individual long hexagonal prism of which the SEM image is shown in Fig. 4b. The ED pattern inset in Fig. 5a indicates that the microprism is of single crystal and can be indexed as the β-$NaGdF_4$ phase, which is in accord with the XRD results in Fig. 1a. The HRTEM image shown in Fig. 5b reveals that the fringe spacing of interlayer is about 0.34 nm, which corresponds well to the distance of the (001) planes. Thus, the preferred growth direction of β-$NaGdF_4$ prisms is along the [001] direction. The growth along [001] direction causes stronger (110) XRD peak in Fig. 1a. The inset of Fig. 5b shows the corresponding FFT image, which presents a 6-fold symmetry and can further confirm the microprism obtained is the high crystallinity of β-$NaGdF_4$.

### 3.3. Crystal growth processes in citric acid and EDTA

The kinetics of the crystal growth process has already been extensively studied in the past decade [7,24–26]. In a word, the difference in the growth rates of various crystal facets results the different morphology of the crystallite. The faster relative rate of growth crystal direction has the smaller the area of crystal facet perpendicular to this growth direction will be.

Shown in Scheme 1a, the small ratio of height to side length demonstrates that the growth rate in the prismatic facets is a little quicker than that top and bottom facets in citric acid condition. As the pH value increases gradually, submicron spheres appeared indicate that sequestering activities of citric acid along all directions are completely uniform. The isotropic growth of crystal is induced. The coordination between the pH value and chelator is important for the morphology of the final products [26]. The hexagonal prisms grown in EDTA show a larger ratio of height to side length than controlled by citric acid. That can be concluded EDTA has the more effective function of enhancement the longitudinal growth along the [001] orientation than citric acid. Furthermore, the spindles appeared demonstrate that the preferential growth orientation is existed which is the [001] direction.

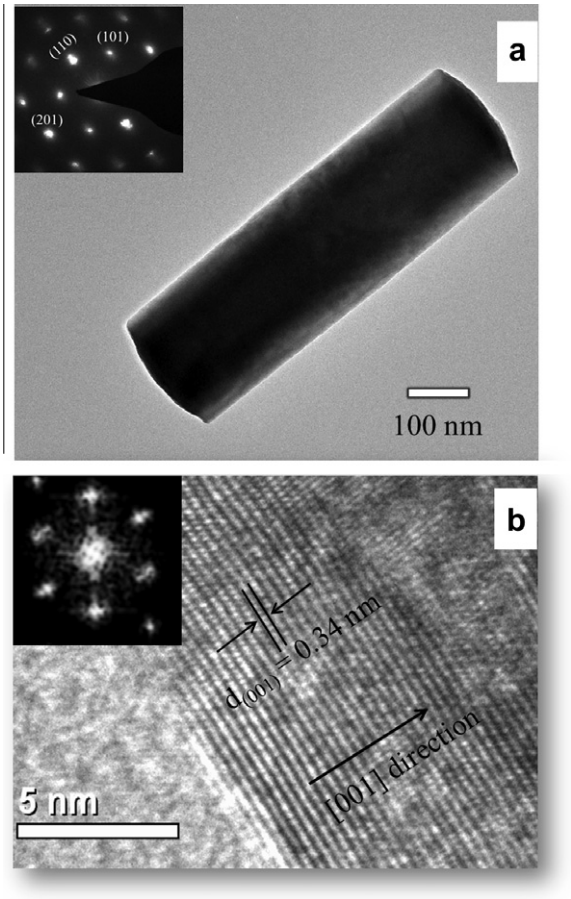


**Fig. 5.** The TEM image, ED pattern, and HRTEM image of long hexagonal prism β-$NaGdF_4$ submicron crystal prepared using EDTA as the chelator.

### 3.4. Luminescence properties

The UCL spectra for the samples synthesized using citric acid and/or EDTA as chelator were recorded upon 980 nm pumping with power of 85 mW/$mm^2$. Fig. 6a and b shows UCL spectra of

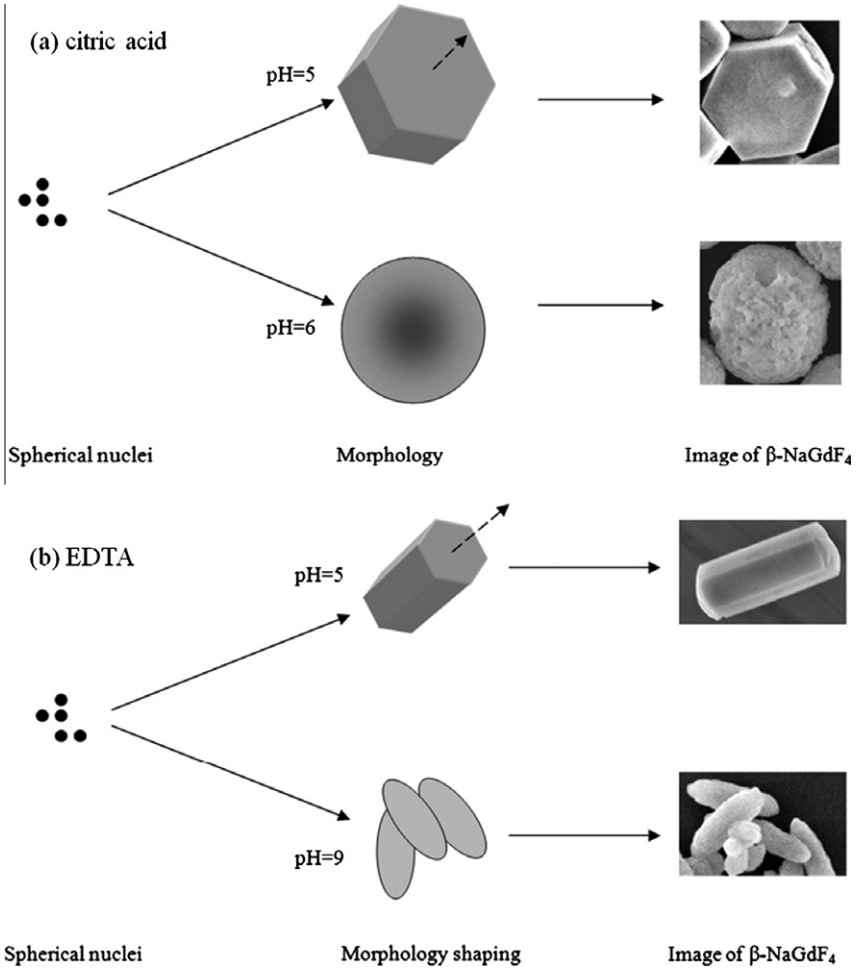


**Scheme 1.** Schematic illustration of β-$NaGdF_4$ crystal growth processes with citric acid (a) and EDTA (b) as the chelators.

β-$NaGdF_4$:(20%)$Yb^{3+}$/(0.3%)$Tm^{3+}$ crystals with the typical morphologies of short hexagonal prisms and spheres synthesized using citric acid as the chelator. Fig. 6c and d shows UCL spectra of the spindles and long hexagonal prisms β-$NaGdF_4$:(20%)$Yb^{3+}$/(0.3%)$Tm^{3+}$ crystals synthesized using EDTA as the chelator. The UCL spectra appear typical emissions of both $Tm^{3+}$ and $Gd^{3+}$ including emissions from $^1I_6$, $^1D_2$ and $^1G_4$ levels of $Tm^{3+}$ and $^6P_J$ levels of $Gd^{3+}$ (shown by the red symbol). Fig. 7 presents the energy level diagrams of $Yb^{3+}$, $Tm^{3+}$, and $Gd^{3+}$ ions [27] and the proposed energy transfer mechanisms [28–30] in $Yb^{3+}$/$Tm^{3+}$ co-doped β-$NaGdF_4$ under 980 nm excitation. It is important to note that the $^6P_J \rightarrow {}^8S_{7/2}$ emission of $Gd^{3+}$ is observed at 310 nm. Due to $Gd^{3+}$ ions cannot be excited by 980 nm directly, there must exist energy transfer from $Tm^{3+}$ to $Gd^{3+}$ [21,31].

Comparing intensities of various morphologies, the emission intensities have enhanced obviously of hexagonal prisms. The prisms have higher crystallinity than nanoparticle-clusters (spheres and spindles) which decrease the defect concentrations, then leading to an enhanced UCL [5,23].

The UCL spectra for different samples show different intensities of up-converted UV emissions originated from $^1I_6 \rightarrow {}^3F_4$ and $^1D_2 \rightarrow {}^3H_6$ transitions relative to the blue UCL originated from $^1G_4 \rightarrow {}^3H_6$ transition of $Tm^{3+}$. The different spectral distributions in UCL spectra for different samples may be resulted from different crystallinities and surface properties rather than the morphologies [5,7,32,33].

To understand the UCL mechanisms, we had measured the pump power dependence of UCL intensities for the long hexagonal prisms sample of which UCL spectrum was shown in Fig. 6d. Fig. 8 shows the double logarithmic plots of the emission intensity as a function of excitation power for the $^1G_4 \rightarrow {}^3H_6$, $^1D_2 \rightarrow {}^3F_4$, and $^1I_6 \rightarrow {}^3F_4$ emissions of long hexagonal prisms. The slope $n$ means the number of NIR photons required to absorb for emitting one up-converted photon [34,35]. Due to the competition between the linear decay and up conversion of the excited states, the $n$ becomes smaller than the theoretical value under high excited pump power [35,36]. But, linear decay is dominant under lower excited pump power which is used in our experiment. For the long hexagonal prisms sample, the n values of $^1G_4 \rightarrow {}^3H_6$, $^1D_2 \rightarrow {}^3F_4$, and $^1I_6 \rightarrow {}^3F_4$ emissions are obtained to be 2.8, 4.5, and 5.6, respectively. The pump power dependence of $^6P_J \rightarrow {}^8S_{7/2}$ transitions of $Gd^{3+}$ is found with the same tendency as $Tm^{3+}$:$^1I_6$, shown in Fig. 8. This indicates that the $^6P_J$ levels of $Gd^{3+}$ are populated via energy transfer from $^1I_6$ level of $Tm^{3+}$ to $^3P_J$ of $Gd^{3+}$.

Combined the slope n and energy diagrams of $Tm^{3+}$ and $Yb^{3+}$, the proposed pathways for upconversion emissions are demonstrated in Fig. 7. The pump laser photons of 980 nm can only excite the $Yb^{3+}$ ions, then three successive energy transfers from $Yb^{3+}$ to $Tm^{3+}$ populate $^3H_5$, $^3F_2$, and $^1G_4$ levels respectively with the redundant energy dissipated by phonons [28,37,39]. Due to the large energy mismatch between $Tm^{3+}$ $^1D_2$–$^1G_4$ and $Yb^{3+}$ $^2F_{5/2}$–$^2F_{7/2}$, the probability of $^1D_2$ populated by the fourth photon from $Yb^{3+}$ via energy transfer to the $^1G_4$ is low. According to previous reports, the cross-relaxations between $Tm^{3+}$ ions play the important role in populating $^1D_2$ level [37,39]. Usually, there are primarily two cross-relaxation processes in populating the $^1D_2$ level:

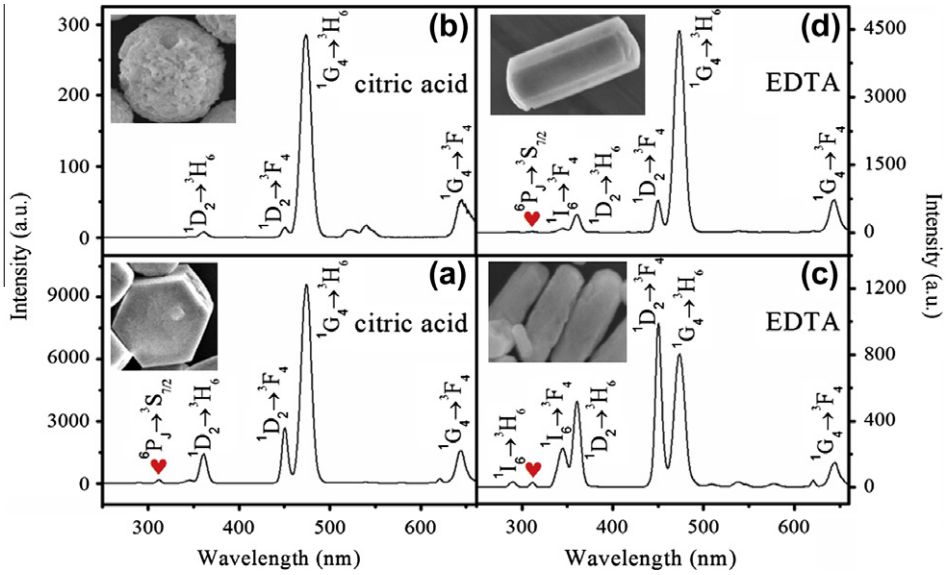


**Fig. 6.** UCL spectra pumped by a 980 nm laser diode with power of 85 mW/mm [2] for β-$NaGdF_4$:(20%)$Yb^{3+}$/(0.3%)$Tm^{3+}$ synthesized using citric acid as the chelator (a and b) for pH value of 5 (a) and 7 (b); and using EDTA as the chelator (c and d) for pH value of 4.5 (c) and 5.1 (d). Insets illustrate SEM images of the samples. All of the samples were hydrothermally treated with the $F^-/Ln^{3+}$ ratio of 12:1.

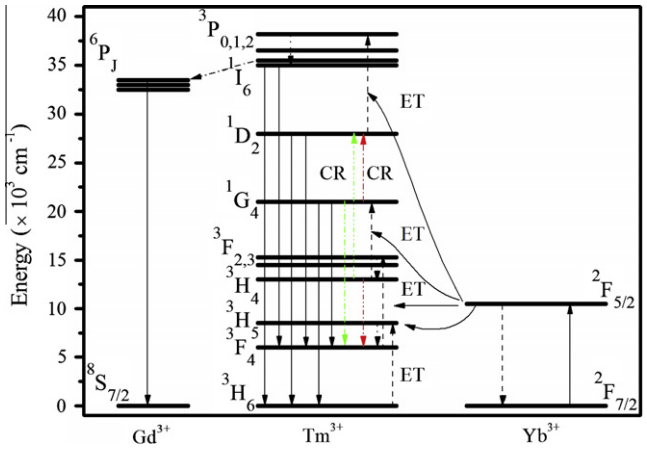


**Fig. 7.** The energy level diagrams and proposed energy transfer pathways for β-$NaGdF_4$:$Yb^{3+}$/$Tm^{3+}$ sample under 980 nm excitation.

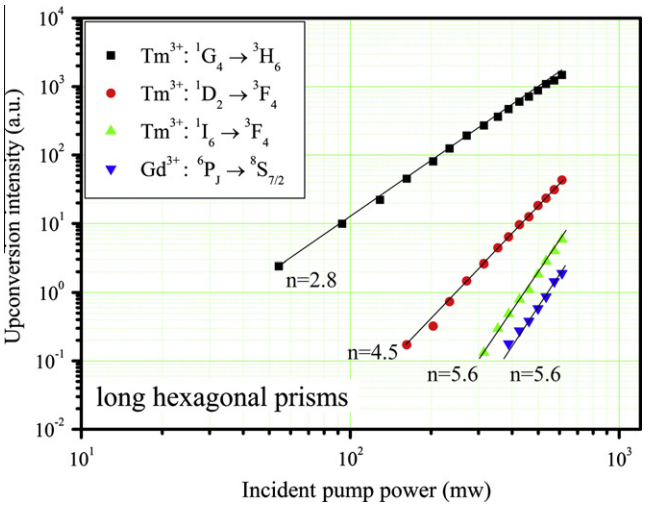


**Fig. 8.** Power dependence of UCL intensities of $^1G_4 \rightarrow {}^3H_6$, $^1D_2 \rightarrow {}^3F_4$ and $^1I_6 \rightarrow {}^3F_4$ emissions of $Tm^{3+}$ and $^6P_J \rightarrow {}^8S_{7/2}$ emission of $Gd^{3+}$ in long hexagonal prisms β-$NaGdF_4$:(20%) $Yb^{3+}$/(0.3%)$Tm^{3+}$ submicron crystals under 980 nm laser diode pump.

$^3H_4 + {}^1G_4 \rightarrow {}^3F_4 + {}^1D_2$ and $^1G_4 + {}^3H_4 \rightarrow {}^3F_4 + {}^1D_2$. After populating the $^1D_2$ state, another energy transfer process from the $Yb^{3+}$ to $Tm^{3+}$ ion excites this state to the $^3P_2$ state, followed by rapidly nonradiative decays to the $^1I_6$ state from which $^1I_6 \rightarrow {}^3H_6$ and $^1I_6 \rightarrow {}^3F_4$ emissions are produced [29]. As sample temperature is higher, this nonradiative relaxation is greatly influenced and competes with the radiative transitions of $^3P_2 \rightarrow {}^3H_6$ and $^3P_2 \rightarrow {}^3F_4$ [38]. But the $^3P_2 \rightarrow {}^3H_6$ and $^3P_2 \rightarrow {}^3F_4$ emissions were not observed in our experiment, even when the excited power increased to 195 mW/mm [2]. Consequently, the UCL from $^1G_4$, $^1D_2$, and $^1I_6$ states are related to three, five, and six photons processes, respectively [29,30].

Submicron-sized β-$NaGdF_4$:(20%)$Yb^{3+}$/(1%)$Ho^{3+}$ crystals had been also synthesized by HT using citric acid and/or EDTA as the chelators, respectively. The synthesis conditions were typically temperature of 180 °C, time of 2 h, pH value of 5, and $F^-/Ln^{3+}$ ratio of 12:1. Fig. 9 shows UCL spectra under 980 nm laser pumping (85 mW/mm$^2$) for β-$NaGdF_4$:(20%)$Yb^{3+}$/(1%)$Ho^{3+}$ submicron crystals synthesized using EDTA (top) and citric acid (bottom). The emission spectra are normalized to the strongest emission centered at 540 nm. As described by energy level diagrams [27] and proposed energy transfer mechanisms in Fig. 9, the green[1] and the red color emissions are observed in the range of 520–560 nm and 620–670 nm which are the most dominant emissions, corresponding to the intra 4f–4f electronic transitions $^5S_2 + {}^5F_4 \rightarrow {}^5I_8$ and $^5F_5 \rightarrow {}^5I_8$ of $Ho^{3+}$ [40,41], respectively. The emission at 485 nm is ascribed to the $^5F_3 \rightarrow {}^5I_8$ [42]. Both spectra are similar, but one can find that the red UCL spectrum in the top is a little stronger than that in the bottom. As indicated in Fig. 9 (inset), the green and red UCL intensities are proportional to the populations of the $^5I_6$ and the $^5I_7$ levels, respectively. The populations of the two levels are strongly governed by the nonradiative relaxation from the $^5I_6$ to the $^5I_7$[40]. The population competition between the two levels affects the red to green intensity ratio in UCL directly. Therefore,

[1] For interpretation of color in Fig. 9, the reader is referred to the web version of this article.

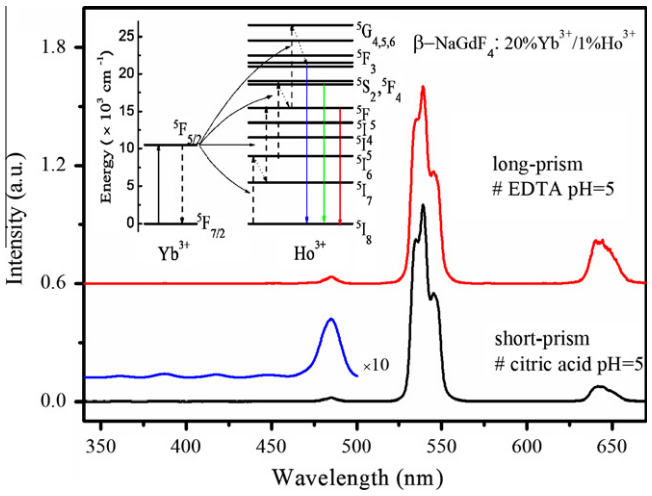


**Fig. 9.** UCL spectra of β-$NaGdF_4$:(20%)$Yb^{3+}$/(1%)$Ho^{3+}$ synthesized using EDTA (top) and citric acid (bottom) as the chelators under 980 nm diode laser pump. UCL intensity is normalized to the strongest emission centered at 540 nm. Inset shows the energy level diagrams and the proposed energy transfer pathways.

increasing the nonradiative relaxation rate could increase the population ratio of the $^5I_7$ to the $^5I_6$ levels, so as to enhance the red UCL of the long hexagonal prisms sample [42]. The upconversion bands observed at 361 nm, 387 nm, 418 nm, and 447 nm are assigned to the transitions from the higher levels $^5G_J$ state to the ground state $^5I_8$ [42]. As the energy transfer pathways show, the upconversion luminescence of the red (centered at 643 nm), green (539 nm), and blue (485 nm) levels is two-photon, two-photon, and three-photon upconversion luminescence, respectively [40,42].

## 4. Conclusion

The single phase β-$NaGdF_4$:$Yb^{3+}$/$Tm^{3+}$ and β-$NaGdF_4$:$Yb^{3+}$/$Ho^{3+}$ submicron crystal phosphors were synthesized using the mild hydrothermal technique by one-step procedure. The synthesis conditions were typically temperature of 180 °C, time of 2 h, and $F^-$/$Ln^{3+}$ ratio of 12:1. The single phase β-$NaGdF_4$:$Yb^{3+}$/$Tm^{3+}$ with the short hexagonal prisms and spheres was formed as pH values in the range of 4.8–9 with the chelator of citric acid. Furthermore, long hexagonal prisms and spindles morphologies could also be obtained with pH values in the range of 4.5–9 using EDTA as the chelator. The results show that citric acid and EDTA have played a different role on the crystal growth. Under 980 nm excitation, the emission bands from $^1G_4$, $^1D_2$, and $^1I_6$ states to the lower lying states of $Tm^{3+}$ were found, which covered all the visible and UV region in β-$NaGdF_4$:$Yb^{3+}$/$Tm^{3+}$, and profoundly one of $^6P_J \rightarrow {}^8S_{7/2}$ transitions of $Gd^{3+}$ around 310 nm was observed implying energy transfer from $Tm^{3+}$:$^1I_6$ to $Gd^{3+}$:$^6P_J$. And, the intense blue of $Tm^{3+}$ and green of $Ho^{3+}$ emissions were bright enough to be observed by naked eye at the lower excitation power (85 mW/mm$^2$). These confirm that the β-$NaGdF_4$ is an proper host for $Ln^{3+}$ doped in the UCL region.

## Acknowledgments

This work was financially supported by the National Nature Science Foundation of China (10834006, 51172226, 10904141, 10904140, 1147278) and the MOST of China (2010AA03A404, 2011AA03A407).

## References

[1] Z. Chen, H. Chen, H. Yu, M.X. Yu, F. Li, Q. Zhang, Z. Zhou, T. Yi, C. Huang, J. Am. Chem. Soc. 130 (2008) 3023.
[2] G.F. Wang, Q. Peng, Y.D. Li, Chem. Commun. 46 (2010) 7528.
[3] J. Zhou, Z. Liu, F.Y. Li, Chem. Soc. Rev. 41 (2012) 1323.
[4] H.P. Liang, N.S. Lawrence, T.G.J. Jones, C.E. Banks, C. Ducati, J. Am. Chem. Soc. 129 (2007) 6068.
[5] Y.J. Sun, Y. Chen, L.J. Tian, Y. Yu, X.G. Kong, Nanotechnology 18 (2007) 275609.
[6] L. Wang, Y. Li, Chem. Mater. 19 (2007) 727.
[7] C.X. Li, Z.W. Quan, J. Yang, P.P. Yang, J. Lin, Inorg. Chem. 46 (2007) 6329.
[8] S. Heer, K. Kömpe, H.U. Güdel, M. Haase, Adv. Mater. 16 (2004) 2102.
[9] J.H. Zeng, J. Su, Z.H. Li, R.X. Yan, Y.D. Li, Adv. Mater. 17 (2005) 2119.
[10] H. Mai, Y. Zhang, R. Si, Z. Yan, L. Sun, L. You, C. Yan, J. Am. Chem. Soc. 128 (2006) 6426.
[11] Z.H. Xu, C.X. Li, P.P. Yang, C.M. Zhang, S.S. Huang, J. Lin, Cryst. Growth Des. 9 (2009) 4752.
[12] J.C. Boyer, L.A. Cuccia, J.A. Capobianco, Nano Lett. 7 (2007) 847.
[13] H.L. Qiu, G.Y. Chen, L. Sun, S.W. Hao, G. Han, C.H. Yang, J. Mater. Chem. 21 (2011) 17202.
[14] F. He, P.P. Yang, D. Wang, N. Niu, S.L. Gai, X.B. Li, Inorg. Chem. 50 (2011) 4116.
[15] Z.L. Wang, J.H. Hao, H.L.W. Chan, J. Mater. Chem. 20 (2010) 3178.
[16] G.Z. Ren, S.J. Zeng, J.H. Hao, J. Phys. Chem. C. 115 (2011) 20141.
[17] J. Zhou, Y. Sun, X.X. Du, L.Q. Xiong, H. Hu, F.Y. Li, Biomaterials 31 (2010) 3287.
[18] Y. Wu, C.X. Li, D.M. Yang, J. Lin, J. Colloid Interface Sci. 354 (2011) 429.
[19] F. Wang, X.P. Fan, M.Q. Wang, Y. Zhang, Nanotechnology 18 (2007) 025701.
[20] C.Y. Cao, W.P. Qin, J.S. Zhang, Opt. Commun. 283 (2010) 547.
[21] C.X. Li, Z.W. Quan, P.P. Yang, S.S. Huang, H.Z. Lian, J. Lin, J. Phys. Chem. C 112 (2008) 13395.
[22] G.S. Yi, H.C. Lu, S.Y. Zhao, Y. Ge, W.J. Yang, D.P. Chen, L.H. Guo, Nano Lett. 4 (2004) 2191.
[23] C. Huang, Coordination Chemistry of Rare Earth Elements, Science Publishing Press, Beijing, 1997.
[24] R.A. Laudise, A.A. Ballman, J. Phys. Chem. 64 (1960) 688.
[25] R.A. Laudise, E.D. Kolb, A.J. Caporaso, J. Am. Ceram. Soc. 47 (1964) 9.
[26] W.J. Li, E.W. Shi, T. Fukuda, Cryst. Res. Technol. 38 (2003) 847.
[27] G.H. Dieke, Spectra and Energy Levels of Rare Earth Ions in Crystals, Wiley-Interscience, Inc., New York, 1968.
[28] F. Auzel, Compt. Rend. 263B (1966) 819.
[29] G.Y. Chen, G. Somesfalean, Z.G. Zhang, Q. Sun, F.P. Wang, Opt. Lett. 32 (2007) 87.
[30] X.R. Hou, S.M. Zhou, H. Lin, H. Teng, Y.K. Li, W.J. Li, T.T. Jia, J. Appl. Phys. 107 (2010) 083101.
[31] W.P. Qin, C.Y. Cao, Opt. Lett. 33 (2008) 2167.
[32] Y.J. Sun, H.J. Liu, X. Wang, X.G. Kong, H. Zhang, Chem. Mater. 18 (2006) 2726.
[33] L. Spanhel, M.A. Anderson, J. Am. Chem. Soc. 113 (1991) 2826.
[34] R.A. Hewes, J.F. Sarver, Phys. Rev. 182 (1969) 427.
[35] M. Pollnau, D.R. Gamelin, S.R. Lüthi, H.U. Güdel, M.P. Hehlen Phys, Rev. B 61 (2000) 3337.
[36] J.F. Suyver, A. Aebischer, S. García-Revilla, P. Gerner, H.U. Güdel, Phys. Rev. B 71 (2005) 125123.
[37] N.K. Giri, S.K. Singh, D.K. Rai, S.B. Rai, Appl. Phys. B 99 (2010) 271.
[38] G.F. Wang, W.P. Qin, L.L. Wang, G.D. Wei, P.F. Zhu, R. Kim, Opt. Express 16 (2008) 11907.
[39] I. Etchart, I. Hernández, A. Huignard, M. Bérard, M. Laroche, W.P. Gillin, R.J. Curry, A.K. Cheetham, J. Appl. Phys. 109 (2011) 063104.
[40] J. Pichaandi, F.C.J.M. van Vegggel, M. Raudsepp, Appl. Mater. Interfaces 2 (2010) 157.
[41] I. Etchart, I. Hernández, A. Huignard, M. Bérard, W.P. Gillin, R.J. Curry, A.K. Cheetham, J. Mater. Chem. 21 (2011) 1387.
[42] G.S. Yi, G.M. Chow, J. Mater. Chem. 15 (2005) 4460.